Depletion of m^{6}A-RNA in *Escherichia coli* reduces the infectious potential of T5 bacteriophage

Bibakhya Saikia[1], Sebastian Riquelme-Barrios[1], Thomas Carell[2], Sophie Brameyer[1*], Kirsten Jung[1*]

[1] Faculty of Biology, Microbiology, Ludwig-Maximilians-Universität München, Martinsried, Germany

[2] Department for Chemistry, Institute for Chemical Epigenetics (ICE-M) Ludwig-Maximilians-Universität München, München, Germany

*Corresponding authors
Prof. Dr. Kirsten Jung
Ludwig-Maximilians-Universität München
Microbiology
Großhaderner Str. 2-4
82152 Martinsried
Phone: + 49 89/2180-74500
Fax: + 49 89/2180-74520
E-Mail: jung@lmu.de

Prof. Dr. Sophie Brameyer
Ludwig-Maximilians-Universität München
Microbiology
Großhaderner Str. 2-4
82152 Martinsried
Phone: + 49 89/2180-74506
Fax: + 49 89/2180-74520
E-Mail: s.brameyer@bio.lmu.de

Keywords: epitransciptome, RNA modification, phage replication, *Vibrio campbellii*, lysogeny, Virtus

Abstract

N^6-methyladenosine (m^6A) is the most abundant internal modification of mRNA in eukaryotes that plays, among other mechanisms, an essential role in virus replication. However, the understanding of m^6A RNA modification in prokaryotes, especially in relation to phage replication, is limited. To address this knowledge gap, we investigated the effects of m^6A RNA modification on phage replication in two model organisms: *Vibrio campbellii* BAA-1116 (previously *V. harveyi* BB120) and *Escherichia coli* MG1655. An m^6A-RNA depleted *V. campbellii* mutant (Δ*rlmF*Δ*rlmJ*) did not differ from the wild type in the induction of lysogenic phages or in susceptibility to the lytic Virtus phage. In contrast, the infection potential of the T5 phage, but not that of other T phages or the lambda phage, was reduced in an m^6A-RNA depleted *E. coli* mutant (Δ*rlmF*Δ*rlmJ*) compared to the wild type. This was shown by a lower efficiency of plaquing and a higher percentage of surviving cells. There were no differences in T5 phage adsorption rate, but the mutant exhibited a 5 min delay in the rise period during the one-step growth curve. This is the first report demonstrating that *E. coli* cells with lower m^6A RNA levels have a higher chance of surviving T5 phage infection.

Importance

The importance of RNA modifications has been thoroughly studied in the context of eukaryotic viral infections. However, their role in bacterial hosts during phage infections is largely unexplored. Our research delves into this gap by investigating the effect of host m^6A-RNA modifications during phage infection. We found that an *E. coli* mutant depleted of m^6A-RNA is more resistant to T5 infection than the wild type. This finding emphasizes the need to further investigate how RNA modifications affect the fine-tuned regulation of individual bacterial survival in the presence of phages to ensure population survival.

Introduction

Chemical modifications of RNA molecules are reversible and dynamic and influence their fate and many cellular processes (1). Of the numerous RNA modifications discovered to date, the eukaryotic m^6A modification machinery and its presence in host and viral RNA are especially well-studied and provide a potential target for antiviral therapeutics (1–7). However, despite the wealth of knowledge regarding m^6A-RNA modification in eukaryotes and eukaryotic viruses, the potential implications of m^6A-RNA modifications in bacteria are limited and in relation to bacteriophages (phages) are still largely unexplored.

Phages are prokaryotic viruses that infect bacteria and use them as hosts to propagate. They are ubiquitous and known to be highly abundant in various natural ecosystems such as soil and water, in addition to the human microbiome (8). Their varied and omnipresent lifecycles reflect their complex interactions with bacterial hosts, which influence their population, virulence and evolution (9). These complex interactions have attracted considerable research interest related to the intricate fine-tuning between hosts and phages. For example, phage-encoded transfer RNAs (tRNAs) are modified like the corresponding host tRNAs, suggesting that they are processed by the same host enzymes (10). Similarly, another study showed that the bacterial toxin CmdT (part of the toxin–antitoxin–chaperone system) acts as an ADP-ribosyltransferase that modifies phage mRNA to block protein translation (11). Thus, as with most eukaryotic viruses, RNA modifications in phages may be performed by host enzymes and may have pro- or anti-viral functions.

Adenosine methylation at the nitrogen (N^6-methyladenosine - m^6A) is present in all types of *Escherichia coli* RNA (12), however, the methyltransferases are only well documented for ribosomal RNA (rRNA) and tRNA. In *E. coli*, 23S rRNA molecules are methylated at nucleotides A1618 and A2030 by RlmF and RlmJ, respectively (13, 14). In addition, the valine-specific tRNA is methylated at nucleotide A37 by TrmM (YfiC) (15). Notable, RlmF is a structural homolog of METTL16, a mRNA methyltransferase in eukaryotes (16). Overexpression of *rlmF* leads to a slight growth defect in *E. coli* (13), whereas deletion of *rlmJ* leads to a higher growth rate under anaerobic conditions (14). Single deletions of either *rlmF* or *rlmJ* do not interfere with ribosome assembly or influence the growth rate in *E. coli* (17). RlmJ is conserved in the phylum Proteobacteria, whereas RlmF is predominantly found in the class *Gammaproteobacteria* (17). Consequently, RlmF, RlmJ and TrmM are well conserved in the marine bacterium *Vibrio campbellii* BAA-1116 (previously known as *Vibrio harveyi* BB120), a model organism for quorum sensing (18). Our previous work with *V. campbellii* has

59 shown the presence of four intact prophages in the *V. campbellii* genome, two of which can be
60 activated under oxidative (mitomycin C) and heat stress (19).

61 To explore the potential role of m^6A-RNA modification in lysogenic and lytic phages, we tested
62 *V. campbellii* and *E. coli* m^6A-RNA depletion mutants lacking both *rlmF* and *rlmJ,* which
63 encode the major m^6A rRNA methyltransferases. We started our study by the induction of
64 lysogenic phages in *V. campbellii* and could show that m^6A modification has no significant
65 effect on the prophage induction. We then searched for lytic phages that showed different
66 infection efficiency in the m^6A-RNA depleted mutants. We identified bacteriophage T5, whose
67 infectious potential was reduced in the m^6A-RNA depleted *E. coli* mutant, resulting in higher
68 host survival.

69

70 ## Results

71 **m^6A-RNA depletion in *V. campbellii* does not affect prophage induction or susceptibility**
72 **to a lytic phage**

73 *V. campbellii* has four intact prophages in its genomes (19). Prophages are viral DNA segments
74 that have integrated into the host genome (also called lysogen) and provide a competitive
75 advantage to the host (20). In *V. campbellii*, ΦHAP-1-like prophage and *Vibrio* kappa-like
76 prophage are triggered into their lytic cycle under oxidative or heat stress (19). Prophage
77 induction triggers a transition from the lysogenic to the lytic cycle, resulting in the activation
78 of dormant viral DNA and subsequent viral replication and host cell lysis. Knowing the effects
79 of oxidative and heat stress on prophage induction in the wild type of *V. campbellii*, we wanted
80 to determine whether the m^6A-RNA depleted mutant (Δ*rlmF*Δ*rlmJ*) shows a different response.
81 Deletion of *rlmF* and *rlmJ* in *V. campbellii,* which encode the two m^6A-specific rRNA
82 methyltransferases, resulted, in a decrease of 96.5 % in m^6A levels of the tRNA-depleted
83 mRNA and rRNA fraction (Fig. 1A).

84 First, we tested the role of m^6A-RNA on lysogeny. We exposed the wild type and the
85 Δ*rlmF*Δ*rlmJ* mutant to mitomycin C and monitored the cell lysis caused by phage release over
86 time. At 2.5 hours after exposure to mitomycin C, a greater extent of cell lysis was observed in
87 the Δ*rlmF*Δ*rlmJ* mutant compared to the wild type, but the effect was not statistically significant
88 (Fig. 1B). In parallel, we developed an assay for the quantification of phage particles. For this
89 purpose, we raised antibodies against two major capsid proteins, one for the Vibrio kappa-like
90 prophage and one for the ΦHAP-1-like prophage (VIBHAR_05027 and VIBHAR_01983).

91 Using an indirect ELISA assay, we found a slightly higher concentration of the capsid protein
92 of the Vibrio kappa-like prophage, indicating a higher release of phage particles from the m^6A-
93 RNA depleted mutant of *V. campbellii* compared to the wild type after exposure to mitomycin C
94 (Fig. 1C) and heat stress (Fig. 1D). Although this difference was restored in the complemented
95 mutant (ΔΔ-compl.), in which the two genes were chromosomally reintegrated (Fig. 1C and D),
96 the effect was not statistically significant. In the untreated cells, a low level of capsid proteins
97 was observed due to spontaneous induction of prophages (Fig.1C and D).

98 Under both oxidative and heat stress, we detected higher levels of the capsid protein of the
99 ΦHAP-1-like prophage, indicating a greater release of phages (Fig. 1C and D). However, we
100 could not detect any difference between the wild type, the m^6A-RNA depleted mutant, or the
101 complemented mutant (Fig. 1C and C).

102 We then tested whether the m^6A-RNA modification has an effect during lytic phage infection
103 (Fig. 1E). The availability of the vibriophage Virtus, which is capable of infecting a broad range
104 of *Vibrio* spp. (including *V. campbellii*) (21), provided the unique opportunity to evaluate its
105 infectivity for *V. campbellii* wild type and its Δ*rlmF*Δ*rlmJ* mutant. We tested the efficiency of
106 plaquing by phage Virtus after infection of exponentially grown *V. campbellii* wild type, its
107 Δ*rlmF*Δ*rlmJ* mutant and the complemented mutant (ΔΔ-compl.). However, infectivity by
108 Virtus was comparable for all three strains (Fig. 1E). We also tested the efficiency of plaquing
109 by phage Virtus after infection of stationary phase cells of the *V. campbellii* strains, but could
110 not detect any difference (data not shown).

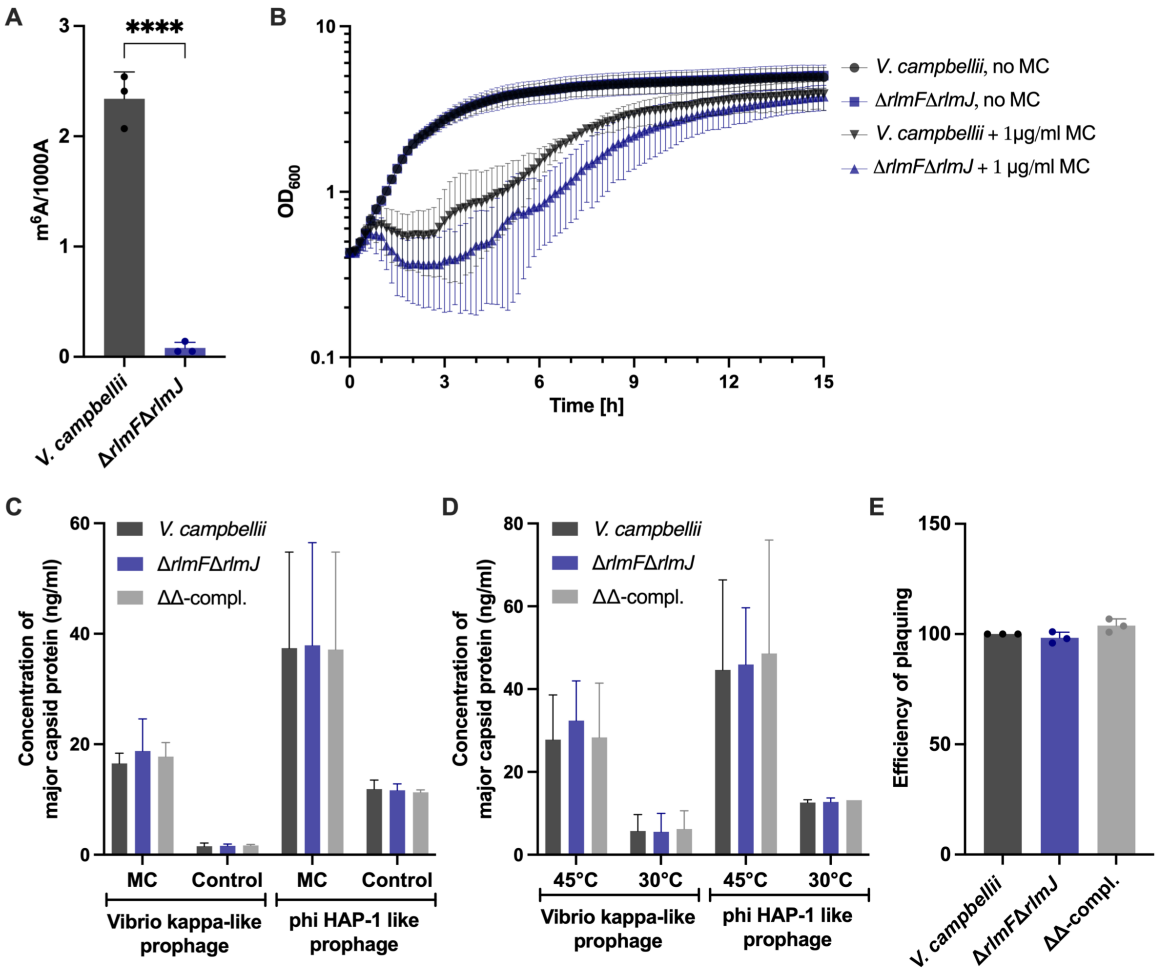

FIG 1 The effect of m^{6}A depletion in *V. campbellii* ATCC BAA1116 on the induction of lysogenic phages and susceptibility to lytic Virtus phage. (A) Quantitative analysis of m^{6}A related to 1000 A (adenosine) of isolated rRNA+mRNA from *V. campbellii* and its Δ*rlmF*Δ*rlmJ* mutant. (B) The indicated strains were grown to the exponential growth phase and exposed to 1 µg/mL mitomycin C (MC) for 30 minutes. Afterwards, cells were resuspended in fresh medium and optical density (OD_{600}) was monitored over time. (C and D) Lysogenic phages were induced in the indicated strains with 1 µg/mL mitomycin C (MC) for 30 minutes (C) or heat at 45°C for 30 minutes (D). Culture supernatants were collected 2 hours after induction and subjected to indirect ELISA to estimate the release of Vibrio kappa-like prophages and ΦHAP-1-like prophages. (E) The indicated strains were grown to the exponential growth phase and infected with phage Virtus. The graph shows the efficiency of plaquing (EOP), which is calculated by dividing the number of plaques obtained from the mutant by the number of plaques obtained from the wild type. The EOP of the wild type was set to 100. Data are presented as the mean ± standard deviation of at least three independent experiments. **** $p < 0.0001$ (Student's *t*-test).

127

128 In summary, the m^{6}A-RNA modification had no effect on prophage induction or replication of
129 the lytic Virtus phage in *V. campbellii.*

130 **m^{6}A-RNA depletion in *E. coli* affects bacteriophage T5 infection**

131 Since further exploration of the role of m^{6}A RNA modification in *V. campbellii* has been
132 hampered by the lack of easily available lytic phages, we proceeded with *E. coli*, which,
133 although containing cryptic prophages in its genome (22), offers a diverse array of well-
134 characterized lytic phages (23). An m^{6}A-RNA depleted mutant (Δ*rlmF*Δ*rlmJ*) *E. coli* MG1655,
135 which has a reduction in the m^{6}A-RNA level comparable to that of *V. campbellii* (Fig. 1A), and
136 a complemented mutant were already available (24).

137

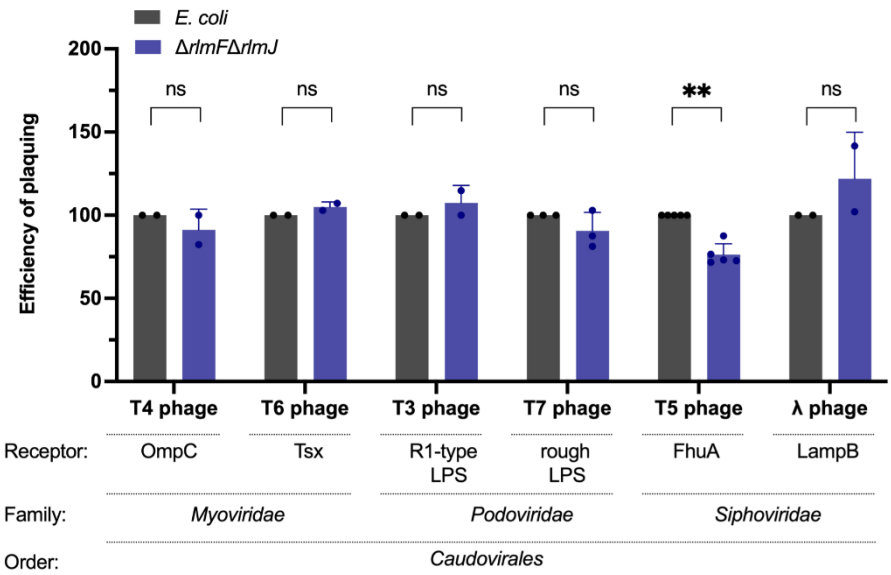

138

139 **FIG 2** Depletion of m^{6}A-RNA in *E. coli* and its effect on infection by different lytic phages. *E. coli* wild
140 type and the Δ*rlmF*Δ*rlmJ* mutant were grown to an OD_{600} = 0.5 before infection with the different
141 phages. The efficiency of plaquing (EOP) was calculated by dividing the number of plaque forming
142 units (PFU) of the Δ*rlmF*Δ*rlmJ* mutant by the number of PFU of the wild type (25). The EOP of the
143 wild type was set to 100. Data are presented as the mean ± standard error of at least two independent
144 experiments. ** $p < 0.01$ (Student's *t*-test). ns, not significant. The primary receptors, phage families
145 and order are indicated below the diagram.

146

147 We screened the most prominent lytic phages for *E. coli,* five of the "T-phages" (23, 26) and
148 the bacteriophage λ (27), for their infection potential of the Δ*rlmF*Δ*rlmJ* mutant compared to

149 the wild type (Fig. 2). All phages tested are double-stranded DNA phages belonging to the order
150 *Caudovirales* and characterized by their tail and icosahedral head (28). They represent three
151 families with different specificity for bacterial host receptors (29) **(**Fig. 2).

152 Of all lytic phages tested, the T5 phage showed significantly reduced plaque formation in the
153 m^6A-RNA depleted Δ*rlmF*Δ*rlmJ* mutant compared to the wild type, an effect that was not found
154 with the other phages (Fig. 2).

155

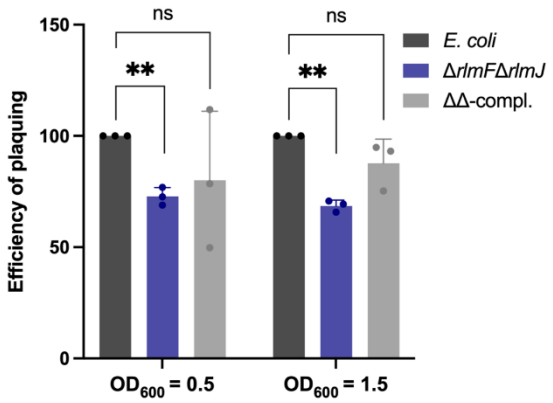

156

157 **FIG 3** The effect of the growth phase of *E. coli* on T5 phage infection. (A and B) *E. coli* wild type, the
158 Δ*rlmF*Δ*rlmJ* mutant and the complemented mutant (ΔΔ-compl.) were infected in the exponential growth
159 phase (OD_{600} = 0.5) (A) or stationary phase (OD_{600} = 1.5) (B). The efficiency of plaquing was calculated
160 as in Fig. 2. Data are presented as the mean ± standard deviation of three independent experiments. **
161 $p < 0.01$ (Student's *t*-test). ns, not significant.

162

163 In a more detailed study, we analyzed the infection by T5 phage at different growth stages of
164 *E. coli* (Fig. 3). The number of plaques was always lower in the Δ*rlmF*Δ*rlmJ* mutant compared
165 to the wild type regardless of the growth phase, an effect that was no longer observed in the
166 complemented mutant (ΔΔ-compl.) (Fig. 3). Thus, the lower infection potential of T5 phage is
167 due to the absence of the m^6A RNA modification.

168 **m^6A-RNA depletion increases survival of *E. coli* after bacteriophage T5 infection**

169 The reduced efficiency of plaquing of bacteriophage T5 found for the Δ*rlmF*Δ*rlmJ* mutant
170 compared to wild-type *E. coli* (Fig. 2 and 3), prompted us to monitor the survival of both strains
171 at different multiplicities of infection (MOI), which represent the ratio of T5 bacteriophage
172 particles to bacterial cells. In the control experiment (Fig. 4A), bacterial cells proliferated and
173 no lysis was observed. However, the addition of T5 phage resulted in lysis of bacterial cells

174 (Fig. 4B to E), confirming that the observed phenomenon was a consequence of phage infection.
175 Infection of the exponentially grown *E. coli* wild type and the m^6A-RNA depleted mutant with
176 T5 phage at an MOI of 10 or 1 led to the complete collapse of both populations, with earlier
177 collapse at an MOI of 10 (Fig. 4B and C). In both strains, the excess of T5 phage led to rapid
178 cell death. Similarly, infection at an MOI of 0.1 resulted in earlier collapse of both populations
179 than at an MOI of 0.01 (Fig. 4D and E). Strain-specific differences during infection with T5
180 phage became evident at an MOI of 0.01 (Fig. 4E). The m^6A-RNA depleted mutant
181 (Δ*rlmF*Δ*rlmJ*) survived approximately 3 hours longer than the wild type before dramatic cell
182 lysis occurred (Fig. 4E). Furthermore, the cells of the mutant population survived the infection
183 better than the wild type, as about twice as many cells were not lysed (Fig. 4E).

184

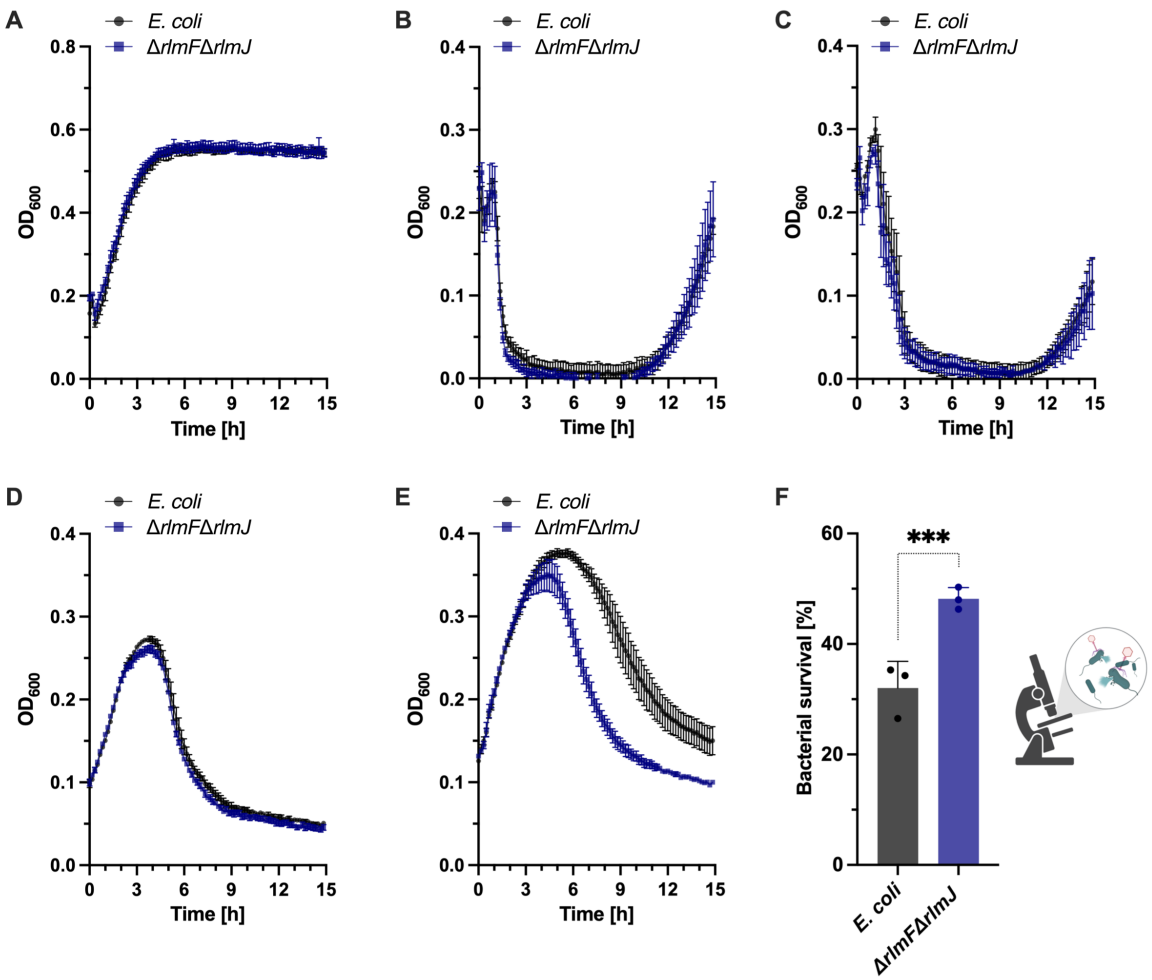

185

186 **FIG 4** Survival of *E. coli* wild type and Δ*rlmF*Δ*rlmJ* mutant after bacteriophage T5 infection at different
187 MOIs. (A-E) *E. coli* wild type and Δ*rlmF*Δ*rlmJ* mutant were grown to exponential growth phase in
188 Nutrient broth. About $2*10^8$ cells (CFUs) were noninfected (A) or infected with T5 phage at MOI of 10
189 (B), 1 (C), 0.1 (D) and 0.01 (E). The mixtures were transferred to 96-well plates (150 µL per well) and
190 the OD_{600} was measured every 10 min at 37 °C with continuous shaking. (F) *E. coli* strains were infected

191 with T5 phage at MOI of 10. Single cells were monitored by phase contrast time-lapse microscopy,
192 imaged every 2 min, and the percentage of surviving cells after 2.5 hours was determined. A total of
193 2,080 wild-type and 1,923 Δ*rlmF*Δ*rlmJ E. coli* cells were quantified at time point 2.5 h post-infection.
194 Data are presented as the mean ± standard error (A-D) or as mean ± standard deviation of the mean (F)
195 of three independent biological replicates.

196

197 In addition, we analyzed the time-dependent lysis of the bacteria after T5 infection using phase-
198 contrast time-lapse microscopy. Exponential phase *E. coli* wild type and Δ*rlmF*Δ*rlmJ* mutant
199 were infected with T5 phage at an MOI of 10 to ensure synchronous phage infection or with
200 nutrient broth as a control. After adsorption for 10 min, samples were spotted on an agarose pad
201 and imaged up to 3 hours post-infection. A significantly higher proportion of cells from the
202 Δ*rlmF*Δ*rlmJ* population survived after 2.5 hours of T5 infection compared to the *E. coli* wild-
203 type population (Fig. 4F). This result is consistent with the survival experiments (Fig. 4E).

204

205 **m^6A-RNA depletion in *E. coli* does not affect T5 phage absorption but diminishes its**
206 **infection potential**

207 To further investigate T5 phage-host interactions, we investigated adsorption of T5 to *E. coli*
208 wild type and Δ*rlmF*Δ*rlmJ* mutant (Fig. 5A). We observed similar adsorption rates of T5 phage
209 to both host strains, with at least 60 % adsorption within 15 min and 85 % adsorption within 25
210 min (Fig. 5A). These results suggest that the higher percentage of surviving cells observed in
211 the m^6A-RNA depleted mutant after T5 phage infection is likely not due to differences in
212 binding to host cells, but is instead related to processes that occur after virus-receptor
213 interaction.

214 To test this, one-step growth curves were performed with the *E. coli* wild type and the
215 Δ*rlmF*Δ*rlmJ* mutant, with the aim to characterize the dynamics of T5 phage replication. In
216 particular, this analysis allowed us to determine (i) the latent period, the time for production of
217 phage components and virion assembly until phage-induced lysis of infected cells, (ii) the rise
218 period, which includes the rise in phage concentration and asynchronous bursts, and (iii) the
219 burst size, a measure of phage virions produced per infected cell (Fig. 5B). For both strains, the
220 latent period was observed to be 45 min, followed by a rise period for another 45 min, followed
221 by a burst period (Fig. 5B). In the Δ*rlmF*Δ*rlmJ* mutant, a significant delay in the increase of the
222 phage titer was observed during the rise period compared to the wild type, which was
223 particularly evident at the 60- and 75-minute time points. This period indicates the rise in phage

224 number due to the release of progeny phage particles by lysis of infected bacterial cells. In
225 addition, the burst size for the *E. coli* wild type was 364 phages compared to 339 phages for the
226 Δ*rlmF*Δ*rlmJ* mutant, a reduction of approximately 7 % per infection cycle. These results
227 suggest that the m^{6}A-RNA depleted mutant releases progressively fewer phages over multiple
228 rounds of infection, explaining the higher survival rates (Fig. 4E and F) and the lower number
229 of PFU in the mutant (Fig. 3).

230

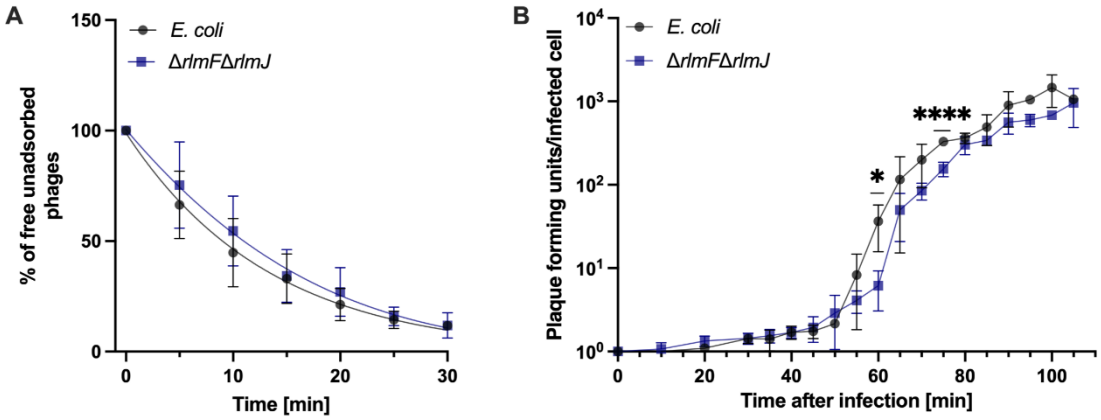

231

232 **FIG 5** Characterization of T5 phage infection in *E. coli* wild type and Δ*rlmF*Δ*rlmJ* mutant. (A)
233 Adsorption kinetics of T5 phage to wild type and m^{6}A-RNA depleted mutant *E. coli* at MOI 0.1. Free
234 phages were collected at the indicated time points after infection (0 min), and the concentration of free
235 phages was determined using plaque assays. (B) One-step growth curve of T5 phage determined for
236 wild type and m^{6}A-RNA depleted mutant at MOI 0.01. Data are presented as the mean ± standard
237 deviation of at least three independent experiments * $p < 0.05$; ** $p < 0.01$; **** $p < 0.0001$ (paired
238 Student´s t-test).

239

240 ## Discussion

241 In eukaryotes, m^{6}A-RNA modifications are crucial for viral infection and host innate antiviral
242 immunity (30). The effect of this modification is highly dependent on the particular virus and
243 cell types involved, leading to either enhancement or inhibition of viral replication in eukaryotes
244 (30).

245 To date, there are only a few examples of RNA related modifications known that are important
246 in the context of phage replication (31). Adenosine diphosphate (ADP)-ribosyltransferases
247 (ARTs) of the T4 phage post-translationally modify host proteins with ADP-ribose from the
248 substrate NAD (32, 33). A recent study reported that one of these enzymes, ModB, accepts not

249 only NAD^+ but also NAD^+-capped RNA as a substrate (34). Thereby, RNA chains are
250 covalently attached to host proteins in a process, called RNAylation. T4 phages with inactive
251 ModB are characterized by delayed lysis and a reduced number of progenies. The first internal
252 mRNA modification has been described by the group of Michael Laub. They found that the
253 ART CmdT modifies the N^6 position of adenine in GA dinucleotides within single-stranded
254 RNAs leading to an arrest of mRNA translation and inhibition of T4 phage replication (11).

255 Here, we found that plaquing efficiency of the T5 phage was significantly reduced in a m^6A-
256 RNA depleted *E. coli* mutant compared to the wild type (Fig. 2 and 3). Consequently, more
257 cells of the mutant survived infection with the T5 phage (Fig. 4). Similarly, the lack of the m^6A
258 reader/writer YTHDF2 and the m^6A writer METTL3 in eukaryotic BSC40 cell lines attenuates
259 the replication of dsDNA simian vacuolating virus 40 (SV40) (35).

260 Since T5 phage efficiently adsorbed to both the wild type and m^6A-RNA depleted mutant of
261 *E. coli* (Fig. 5A), the greater bacterial survival of the mutant likely resulted from changes during
262 the steps after virus receptor interaction. The one-step growth curve showed a 5-min delay in
263 the rise period of the m^6A-RNA depleted mutant, which was particularly significant at the 60-
264 and 75-min time points (Fig. 5B). This slight delay in the rise period during T5 phage infection
265 may indicate a delay in phage assembly and/or host cell lysis. Strikingly, when analyzing the
266 behavior of single cells, we observed a substantial diversification of the population during T5
267 phage infection. A larger proportion of m^6A-RNA depleted cells survived the infection
268 compared to the wild type. In addition, approximately 30% of wild-type cells resisted lysis
269 (Fig. 4F). We hypothesize that the degree of m^6A-RNA modification of *E. coli* is heterogeneous
270 and fine-tunes the infection of individual cells by the T5 phage.

271 In this study, it was shown for the first time that m^6A-RNA modification of *E. coli* fine-tunes
272 the replication of T5 bacteriophage. Host cells with lower m^6A levels have a higher chance of
273 surviving phage infection. We hypothesize that a heterogeneous m^6A modification level in
274 individual cells of the *E. coli* population provides a survival advantage because a subset of the
275 population with lower m^6A modification levels can escape phage infection and lysis.

276

277

278 # Materials and methods

279 ## Strains, plasmids and oligonucleotides

280 The bacterial strains, bacteriophage strains and plasmids used in this study are listed in Table
281 1. Oligonucleotide sequences are listed in Table 2.

282 Table 1: Bacterial strains, bacteriophages and plasmids used in this study

Strain	**Genotype**	**Reference**
V. campbellii ATCC BAA-1116	*V. campbellii* wild type	(18)
V. campbellii Δ*rlmJ*	Deletion of *rlmJ* in *V. campbellii*	This work
V. campbellii Δ*rlmF*Δ*rlmJ*	Deletion of *rlmJ* and *rlmF* in *V. campbellii*	This work
V. campbellii Δ*rlmF*Δ*rlmJ* +	Insertion of *rlmJ* in *V. campbellii* Δ*rlmF*Δ*rlmJ*	This work
V. campbellii ΔΔ-compl.	Insertion of *rlmF* in the *glmS* region of *V. campbellii* Δ*rlmF*Δ*rlmJ*+	This work
V. harveyi VH2	GenBank: LGYS00000000	(36)
E. coli WM3064	*thrB*1004 *pro thi rpsL hsdS lacZ*ΔM15 RP4-1360 Δ(*araBAD*)567 Δ*dapA*1341::[*erm pir*]	W. Metcalf, Univ. of Illinois, Urbana
E. coli BL21 (DE3)	F^- *ompT gal dcm lon* $hsdS_B$ (r_B^- m_B^-) λ(DE3)	(37)
E. coli DH5αλpir	*endA1 hsdR17 glnV44* (= *supE44*) *thi-1 recA1 gyrA96 relA1* φ80d*lac*Δ(*lacZ*)M15 Δ(*lacZYA-argF*)U169 *zdg*-232::Tn10 *uidA*::*pir*+	(38)
E. coli MG1655	K-12 F^- λ^- *ilvG*$^-$ *rfb-50 rph-1*	(22)
E. coli MG1655Δ*rlmF*Δ*rlmJ*	Deletion of *rlmJ* and *rlmF* in *E. coli*	(24)
E. coli MG1655 ΔΔ-compl.	Insertion of *rlmF* and *rlmJ* in *E. coli* Δ*rlmF*Δ*rlmJ*	(24)
E. coli strain B	DSM 613	German Collection of Microorganisms and Cell Cultures GmbH (DSMZ)
E. coli DSM 4230	DSM 4230	(39)
Bacteriophage strain	**Identifier**	**Source**
Virtus phage	GenBank: OK381870	(21)
T3 phage	DSM 4621; GenBank: NC_047864.1	German Collection of Microorganisms and Cell Cultures GmbH (DSMZ)

T4 phage	DSM 4505; GenBank: AF158101.6	German Collection of Microorganisms and Cell Cultures GmbH (DSMZ)
T5 phage	DSM 16353; GenBank: AY543070.1	German Collection of Microorganisms and Cell Cultures GmbH (DSMZ)
T6 phage	DSM 4622; GenBank: MH550421.1	German Collection of Microorganisms and Cell Cultures GmbH (DSMZ)
T7 phage	DSM 4623; GenBank: NC_001604.1	German Collection of Microorganisms and Cell Cultures GmbH (DSMZ)
λ(lambda)phage	DSM 4499; GenBank: J02459.1	German Collection of Microorganisms and Cell Cultures GmbH (DSMZ)
Plasmid	**Genotype**	**Reference**
pNTPS138-R6KT	*mobRP4*$^{+}$ *ori*-R6K *sacB*; suicide plasmid for in-frame deletions, Km^R	(40)
pNPTS138-R6KT-KO-*rlmF*	pNPTS-138-R6KT-derived suicide plasmid for in-frame deletion of *rlmF* in *V. campbellii,* Km^R	This work
pNPTS138-R6KT-KO-*rlmJ*	pNPTS-138-R6KT-derived suicide plasmid for in-frame deletion of *rlmJ* in *V. campbellii,* Km^R	This work
pNPTS138-R6KT-KI-*rlmJ*	pNPTS-138-R6KT-derived suicide plasmid for insertion of *rlmJ* in *V. campbellii* Δ*rlmF*Δ*rlmJ,* Km^R	This work
pNPTS138-R6KT-*glmS*flank-*rlmF*-KI	pNPTS-138-R6KT-derived suicide plasmid for insertion of *rlmF* in the *glmS* region in *V. campbellii* Δ*rlmF*Δ*rlmJ* +, Km^R	This work
pET28a	Expression vector, Km^R	Novagen
pET28a-V05027	N-terminal His_6-tagged *VIBHAR_05027, phage major capsid protein* under the control of the T7 promoter, Km^R	This work
pET28a-V01983	N-terminal His_6-tagged *VIBHAR_01983, phage major capsid protein* under the control of the T7 promoter, Km^R	This work

Table 2: Primers used in this study.

Name	Sequence
rlmF_FL_up_fwd	5‘-ctggcgccaagcttctctgcaggatgagaaacctaagatgaaagtcttgc-3‘
rlmF_FL_OL_rev	5‘-ctttaattcaatccaggctttgcgcgcgttgtgattattggtcttcatt-3‘
rlmF_FL_OL_fwd	5‘-aatgaagaccaataatcacaacgcgcgcaaagcctggattgaattaaag-3‘
rlmF_FL_down_rev	5‘-gaagctagcgaattcgtggatccagatggctttcagaggcaaaaatcatggc-3‘
rlmJ_FL_up_fwd	5‘-ctggcgccaagcttctctgcaggatctggtccagcttgggtttgcgttg-3‘
rlmJ_FL_OL_rev	5‘-tattcaggaacgatccagtcgactttgaagctgtggcggtaacttaacaaa-3‘
rlmJ_FL_OL_fwd	5‘-tttgttaagttaccgccacagcttcaaagtcgactggatcgttcctgaata-3‘
rlmJ_FL_down_rev	5‘-agctagcgaattcgtggatccagatgaagaacttggtttcaccagacag-3‘
M13_rev	5‘-caggaaacagctatgacc-3‘
M13_uni	5‘-tgtaaaacgacggccagt-3‘
rlmJ_check_F	5‘-gaccaaatgcggctcaagc-3‘
rlmJ_check_R	5‘-gctttgacgatggcagcacg-3‘
rlmF_check_F	5‘-gtgggcatttgtctttgac-3‘
rlmF_check_R	5‘-caattgaccaatcttggcg-3‘
pNPTS_glmS_Fwd	5′- ctggcgccaagcttctctgcaggatgccgcagcaaatcaacgcagcgctg-3′
glmS_rlmF_Rev	5′- gactttcatcttaggtttctcaaaaaagcgaagtcatgtgacttcg-3′
rlmF_glmS_Fwd	5′-gtaattatttagagaaagctatacccgtatatctactgacattgttatcttgttatac-3′
glmS_pNPTS_Rev	5′- gctagcgaattcgtggatccagatcatcaacgaaaccgagatcattgag-3′
glmS_rlmF_Fwd	5′-cgaagtcacatgacttcgctttttgagaaacctaagatgaaagtc-3′
rlmF_glmS_Rev	5′-gtataacaagataacaatgtcagtagatatacgggtatagctttctctaaataattac-3′
VC_glmS_check_F	5′- gccttcacgactcagctctc-3′
VC_glmS_check_R	5′- cgagacactttacaaccaac-3′
V05027-EcoRI-fwd	5′-tagccgaattcatgcttaatgccgtatcgactc-3′
V05027-Xhol-rev	5′-tagccctcgagttacccttcgcagattcaacaacg-3′
V01983-EcoRI-fwd	5′-tagccgaattcatgcctgataattacaccactcg-3`
V01983-Xhol-rev	5′-tagccctcgagttaaccgactttgacgacaacaa-3′
pET28a_check_F	5′-aagtggcgagcccgatcttcc-3′
pET28a_check_R	5′-gatatagttcctcctttcagc-3′

Plasmid and bacterial strain construction

Molecular methods were carried out according to the manufacturers' instructions. Chromosomal DNA isolation, plasmid isolation and PCR product clean-up kits were purchased from Süd-Laborbedarf Gauting (SLG) (Gauting, Germany). Enzymes and HiFi DNA Assembly Master Mix were purchased from New England BioLabs (Ipswich, MA, USA).

Construction of the marker-less double deletion mutant *V. campbellii* Δ*rlmF*Δ*rlmJ* was achieved using the suicide plasmids pNPTS138-R6KT-KO-*rlmJ* and pNPTS138-R6KT-KO-*rlmF*. Briefly, 600-bp regions upstream and downstream of *rlmJ* or *rlmF* were amplified by PCR using genomic DNA from *V. campbellii* as a template. The primers rlmJ_FL_up_fwd and rlmJ_FL_OL_rev were used for the upstream fragment of *rlmJ;* rlmJ_FL_OL_fwd and rlmJ_FL_down_rev rev for the downstream fragment of *rlmJ*; rlmF_FL_up_fwd and rlmF_FL_OL_rev for the upstream fragment of *rlmF*; and rlmF_FL_OL_fwd and

298 rlmF_FL_down_rev for the downstream fragment of *rlmF*. After purification, the PCR
299 fragments were cloned by Gibson assembly (41) into the suicide plasmid pNPTS138-R6KT,
300 which was first linearized by digestion with EcoRV. The correct plasmids were verified by
301 colony PCR and sequencing using primers M13_rev and M13_uni.

302 The suicide plasmid pNPTS138-R6KT-KO-*rlmJ* was next introduced into wild-type
303 *V. campbellii* by conjugative mating using *E. coli* WM3064 as a donor in LB medium
304 containing diaminopimelic acid (DAP) as previously described (42). Briefly, single-crossover
305 integration mutants were selected on LM plates that contained kanamycin but lacked DAP.
306 Single colonies were grown for two days without antibiotics and plated on LB containing 10%
307 (w/v) sucrose to select for plasmid excision. Kanamycin-sensitive colonies were checked for
308 gene deletion by colony PCR using primers bracketing the deletion sites. Deletion of *rlmJ* was
309 verified by colony PCR and sequencing using the primers rlmJ_check_F and rlmJ_check_R.
310 *rlmF* was then deleted through the introduction of the suicide plasmid pNPTS138-R6KT-KO-
311 *rlmF* into *V. campbellii* Δ*rlmJ* via conjugative mating using *E. coli* WM3064 as a donor as
312 described above. Deletion of *rlmF* was verified by colony PCR and sequencing using the
313 primers rlmF_check_F and rlmF_check_R.

314 Complementation of the *rlmJ* deletion in *V. campbellii* Δ*rlmF*Δ*rlmJ* was achieved with the
315 suicide plasmid pNPTS138-R6KT-KI-*rlmJ*. Briefly, *rlmJ* and 600-bp upstream and
316 downstream flanking regions were amplified by PCR using genomic DNA
317 from *V. campbellii* as a template and the primers rlmJ_FL_up_fwd and rlmJ_FL_down_rev.
318 After purification, the 2030-bp long PCR fragment was cloned by Gibson assembly (41) into
319 the suicide plasmid pNPTS138-R6KT, which was linearized by digestion with EcoRV. The
320 correct plasmids were verified by colony PCR and sequencing using primers M13_rev and
321 M13_uni. Construction of the suicide plasmid pNPTS138-R6KT-*glmS*flank-*rlmF*-KI was
322 slightly different due to the presence of transposable elements in the vicinity of the gene.
323 Briefly, the regions surrounding *glmS* and *rlmF* (600 bp upstream and 24 bp downstream) were
324 amplified to generate the suicide plasmid pNPTS138-R6KT-*glmS*flank-*rlmF* using *V.*
325 *campbellii* genomic DNA as a template. Primer pairs used for amplification of *glmS* overhang
326 fragments were pNPTS_glmS_Fwd and glmS_rlmF_Rev (upstream of *rlmF*) and
327 rlmF_glmS_Fwd and glmS_pNPTS_Rev (downstream from *rlmF*). The primers
328 glmS_rlmF_Fwd and rlmF_glmS_Rev were used to amplify *rlmF*. These DNA fragments were
329 assembled via Gibson assembly (41) into the pNPTS138-R6KT plasmid linearized with
330 EcoRV. The plasmid was verified by colony PCR and sequencing using primers M13_rev and
331 M13_uni.

332 To complement Δ*rlmF*Δ*rlmJ*, the suicide plasmid pNPTS138-R6KT-KI-*rlmJ* was introduced
333 into *V. campbellii* Δ*rlmF*Δ*rlmJ* by conjugative mating using *E. coli* WM3064 as a donor in LB
334 medium containing DAP as described above. Insertion of *rlmJ* was verified by colony PCR and
335 sequencing using the primers rlmJ_check_F and rlmJ_check_R. *rlmF* was then added via
336 introduction of suicide plasmid pNPTS138-R6KT-*glmS*flank-*rlmF*-KI to *V. campbellii*
337 Δ*rlmF*Δ*rlmJ*+ by conjugative mating with *E. coli* WM3064 as described above. Insertion of
338 *rlmF* in the *glmS* region of *V. campbellii* was verified by colony PCR and sequencing using the
339 primers VC_glmS_check_F and VC_glms_check_R.

340 To generate plasmids encoding N-terminal 6His-tagged versions of major capsid proteins from
341 *Vibrio* kappa-like prophage and ΦHAP-1-like prophage (*VIBHAR_05027* and *VIBHAR_01983,*
342 respectively), *V. campbellii* genomic DNA was used as a template with primers V05027-EcoRI-
343 fwd and V05027-Xhol-rev (*VIBHAR_05027*) or V01983-EcoRI-fwd and V01983-Xhol-rev
344 (*VIBHAR_01983*). These two genes were cloned into the pET-28a vector using EcoRI and XhoI
345 as restriction sites; the presence of the correct insert was confirmed by colony PCR and
346 sequencing using primers pET28a_check_F and pET28a_check_R.

347 **Mass spectrometry (MS) analysis of mRNA and rRNA methylation in *V. campbellii***

348 To identify m^6A methylation of the rRNA and mRNA moieties in wild type and Δ*rlmF*Δ*rlmJ*
349 mutant *V. campbellii*, total RNA was isolated and processed as previously described (12). In
350 brief, *V. campbellii* cells were grown to an optical density at 600nm (OD_{600}) of 1 and harvested
351 by centrifugation. Total RNA was isolated and tRNA was removed by size exclusion
352 chromatography, resulting in a fraction containing mRNA and rRNA moieties. This RNA
353 fraction was hydrolyzed and quantitatively analyzed by liquid chromatography-tandem MS
354 (LC-MS/MS) (12).

355 **Overproduction and purification of recombinant phage capsid proteins**

356 *E. coli* BL21 (DE 3) was transformed with the vectors pET28a-V05027 and pET28a-V01983
357 to overexpress the major capsid proteins of *Vibrio* kappa-like prophage and ΦHAP-1-like
358 prophage, respectively. Cells were cultivated in LB supplemented with kanamycin (50 mg/mL)
359 at 37 °C to an OD_{600} of 0.5. Isopropyl-β-D-1-thiogalactopyranoside (IPTG) (0.5 mM) was
360 added to the culture to induce *VIBHAR_05027* or *VIBHAR_01983* expression at 37 °C for 2.5
361 h. Cells were harvested (5000 × *g*, 20 min, 4 °C), resuspended, and disrupted in ice-cold
362 disruption buffer (50 mM Tris-HCl [pH 7.5], 10% (v/v) glycerol, 10 mM magnesium chloride,
363 1 mM dithiothreitol, 0.5 mM phenazine methosulfate [PMSF], 3 mg DNase and 100 mM NaCl)

364 using a high-pressure cell disrupter (Constant Systems Limited, Daventry, UK). Cell debris and
365 intact cells were removed by centrifugation (5000 × *g*, 20 min, 4 °C) and the pellet was
366 solubilized in 6 M urea and 10 mM Tris-HCl (pH 7.5) overnight with shaking at 4 °C. Any
367 precipitates or unsolubilized aggregates were removed by ultracentrifugation (20,000 × *g*, 15
368 min, 4 °C) and the supernatant was loaded onto a Ni-nitrilotriacetic acid (NTA) column
369 (Qiagen, Hilden, Germany). After a washing step (6 M urea, 10 mM Tris-HCl [pH 7.5] and 40
370 mM imidazole), the recombinant protein was eluted with elution buffer (6 M urea, 10 mM Tris-
371 HCl [pH 7.5] and 200 mM imidazole).

372 **Generation of polyclonal rabbit antibodies against recombinant phage capsid proteins**

373 Customized polyclonal rabbit antibodies against 6His-VIBHAR_05027 and 6His-
374 VIBHAR_01983 were purchased from Kaneka Eurogentec (Seraing, Belgium). Heterologously
375 produced and purified 6His-VIBHAR_05027 or 6His-VIBHAR_01983 were used as antigens
376 in a Speedy 28-day Immunization Program with two rabbits per antigen as hosts. The specificity
377 of the polyclonal antibodies against 6His-VIBHAR_05027 and 6His-VIBHAR_01983 was
378 verified by western blot analysis as described below.

379 **Sodium dodecyl sulphate-polyacrylamide gel electrophoresis (SDS-PAGE) and western**
380 **blot analysis of 6His-VIBHAR_05027 and 6His-VIBHAR_01983**

381 *SDS-PAGE* (43). Stacking gels consisted of 4% (w/v) acrylamide (in 50 mM Tris [pH 6.8]) and
382 resolving gels of 12.5% (w/v) acrylamide (in 300 mM Tris [pH 8.8]) and were run in a Tris-
383 glycine buffer (25 mM Tris, 192 mM glycine, 0.1% [w/v] SDS [pH 8.3]). Gels were stained
384 overnight in Coomassie staining solution (0.25% [w/v] Coomassie Brilliant Blue R-250, 9.2%
385 [v/v] concentrated acetic acid and 45.4% [v/v] ethanol) and destained in destaining solution
386 (10% [v/v] acetic acid and 40% [v/v] ethanol).

387 *Western blot analysis.* Proteins were transferred to a nitrocellulose membrane using the Trans-
388 Blot Turbo Transfer System (Bio-Rad, Hercules, CA, USA) and then blocked with 5% (w/v)
389 milk powder prepared in Tris-buffered saline (TBS) (pH 7.6) containing 0.1% (v/v) Tween-20
390 (TBST) for 1 h at room temperature. 6His-VIBHAR_05027 and 6His-VIBHAR_01983 were
391 detected by incubating the membrane in TBST with primary polyclonal antibodies (Kaneka
392 Eurogentec, Seraing, Belgium) or primary monoclonal antibodies against the 6His-tag (Thermo
393 Fisher Scientific, Waltham, MA, USA). Membranes were then incubated with the alkaline
394 phosphatase-conjugated goat anti-rabbit IgG (Thermo Fisher Scientific, Waltham, MA, USA)
395 and developed using substrate solution (50 mM sodium carbonate buffer [pH 9.5], 0.1% [w/v]

396 nitroblue tetrazolium and 5 mg/mL 5-bromo-4-chloro-3-indolyl phosphate). PageRuler
397 Prestained Protein ladder (10-180 kDa) (Thermo Fisher Scientific, Waltham, MA, USA) was
398 used as a size standard ladder.

399 **Phage induction assays**

400 Wild type, Δ*rlmF*Δ*rlmJ* mutant and complemented mutant (ΔΔ-compl.) *V. campbellii* were
401 exposed to stress conditions to assess the effect of m^6A RNA modification on prophage
402 induction. Bacterial strains grown in LM medium to an OD_{600} of 0.4 were exposed to either
403 oxidative stress (by addition of 1 µg/mL mitomycin C), heat stress (45 °C) or neither (control).
404 After 30 min of oxidative stress, mitomycin C was removed from the sample by centrifugation
405 (5000 × *g*, 10 min, 4 °C) and the pellet was resuspended in fresh, pre-warmed LM medium.
406 After 30 min of heat stress, the samples were shifted to 30 °C. After 2 h of incubation under
407 physiological conditions, the supernatant containing the phage particles was collected (5000 ×
408 *g*,15 min, 4 °C), passed through a 0.22 µm Millipore Steriflip Vaccum filter (MilliporeSigma,
409 Burlington, MA, USA) and stored at 4 °C.

410 To follow cell lysis caused by the release of lysogenic phages, wild type, Δ*rlmF*Δ*rlmJ* mutant
411 and complemented mutant (ΔΔ-compl.) *V. campbellii* were exposed to 1 µg/mL mitomycin C
412 after strains were grown in LM medium to an OD_{600} of 0.4. After 30 min of oxidative stress,
413 mitomycin C was removed from the sample by centrifugation (5000 × *g*, 10 min, 4 °C) and the
414 pellet was resuspended in fresh, pre-warmed LM medium. The mixtures were transferred to 96-
415 well plates (150 µL per well) and optical density (OD_{600}) was measured every 10 min using a
416 NanoQuant Infinite M200PRO plate reader (Tecan, Männedorf, Switzerland) at 37 °C with
417 continuous shaking.

418 **Indirect enzyme-linked immunosorbent assay (ELISA)**

419 Indirect ELISA was performed according to described protocols (44, 45) with slight
420 modifications for the detection of the major capsid proteins of *Vibrio* kappa-like and ΦHAP-1-
421 like prophages from *V. campbellii*. In brief, 96-well F-bottom, polystyrene, chimney well,
422 black, medium binding microplates (Greiner Bio-One GmbH, Kremsmünster, Austria) were
423 coated with 100 µL of supernatant (derived from the phage induction assays described above)
424 and 0.05 M carbonate buffer (pH 9.6) and then incubated overnight at 4 °C. After washing three
425 times with TBST, each well of the plate was blocked with 200 µL of 5% (w/v) milk powder
426 prepared in TBST for 1 h at 30 °C. After washing three times with TBST, 100 µL of
427 VIBHAR_05027- or VIBHAR_01983-positive serum in 5% (w/v) milk powder with TBST was

428 added to each well and the plate was incubated for 1 h at 30 °C. After three washes with TBST,
429 100 µL of alkaline phosphatase-conjugated goat anti-rabbit IgG (Thermo Fisher Scientific,
430 Waltham, MA, USA) diluted in 5% (w/v) milk powder in TBST was added to each well,
431 followed incubation at 30 °C for 1 h and five washes with TBST. Subsequently, 100 µL of the
432 substrate para-nitrophenyl phosphate (PNPP) (Thermo Fisher Scientific, Waltham, MA, USA)
433 was added to each well and incubated for 30 min in the dark. Last, 50 µL of 2 N sodium
434 hydroxide was added to each well to stop the reaction. The absorbance was immediately
435 measured at 405 nm in a NanoQuant Infinite M200PRO plate reader (Tecan, Mäannedorf,
436 Switzerland). All samples were analyzed in technical duplicates.

437 Standard curves generated with purified major capsid proteins were included in each ELISA
438 run to estimate the concentration of the two major capsid proteins in the sample.

439 **Propagation and determination of phage titer using plaque assay**

440 To obtain high-titer phage stocks, propagation of all phages mentioned in this work was
441 performed using the plate lysate method as described (46). The propagation host used for Virtus
442 phage was *V. harveyi* VH2; the λ phage host was *E. coli* DSM 4230; and the host for all T-
443 phages was *E. coli* B strain (DSM 613).

444 To determine the phage titer, a double agar overlay plaque assay was performed as described
445 (47). In brief, 100 µL of exponential-phase bacterial culture was mixed with 100 µL of diluted
446 phages in soft agar, which was then poured onto a solid medium. The plates were incubated
447 overnight and the number of plaques formed was counted to determine the titer.

448 **Efficiency of plaquing (EOP)**

449 EOP was determined after performing the plaque assay described above, using phage lysates to
450 infect wild type and Δ*rlmF*Δ*rlmJ* mutants of *V. campbellii* and *E. coli*. The EOP was calculated
451 by dividing the number of plaque forming units (PFU) of the Δ*rlmF*Δ*rlmJ* mutant by the number
452 of PFU of the wild type (25). The EOP of the wild type was set to 100.

453 **Bacterial survival after T5 phage infection**

454 *E. coli* wild type and Δ*rlmF*Δ*rlmJ* mutant were grown to exponential growth phase in Nutrient
455 broth (N7519, Sigma-Aldrich, St. Louis, MO, USA). Cells (about $2*10^8$ colony forming units
456 [CFU]/mL) were infected with T5 phage at a multiplicity of infection (MOI) of 10, 1, 0.1 or
457 0.01 to monitor host dynamics. Mixtures were transferred to 96-well plates (150 µL per well)

458 and optical density (OD_{600}) was measured every 10 min using a NanoQuant Infinite M200PRO
459 plate reader (Tecan, Männedorf, Switzerland) at 37 °C with continuous shaking.

460 **Synchronized infection assay**

461 The synchronized infection assay was performed as previously described (48, 49). *E. coli* wild
462 type and Δ*rlmF*Δ*rlmJ* mutant were grown as described above and infected with T5 phage at a
463 MOI of 10. Samples were collected at 0 min and 5 min after infection and immediately plated
464 for CFU enumeration. Three biologically independent infection experiments showing a CFU
465 reduction of at least 95% within 5 min of infection were considered as synchronized infection.

466 **Time-lapse phase contrast microscopy**

467 Phase-contrast time-lapse microscopy was used to follow T5 phage-mediated bacterial lysis
468 using a modified protocol described by Mandal and colleagues (50). *E. coli* wild type and
469 Δ*rlmF*Δ*rlmJ* mutant were grown as described above and infected with T5 phage at a MOI of
470 10 (or with an equal volume of phage diluent as a control). After a 10 min incubation for initial
471 adsorption at 37 °C under agitation, 2 µL of cells were spotted on pads composed of Nutrient
472 broth (N7519, Sigma-Aldrich, St. Louis, MO, USA) and 1% (w/v) agarose. These pads were
473 placed on microscopic slides and covered with a coverslip. Within 20 minutes, images were
474 taken on a Leica DMi8 inverted microscope equipped with a Leica DFC365 FX camera
475 (Wetzlar, Germany). Microscopic phase-contrast images were captured every two min in
476 several positions up to 3 h with a constant temperature of 37 °C using an incubator (PeCon,
477 Erbach, Germany) around the DMi8 microscope. To set the focus plane, automatic autofocus
478 was performed at every position and every time point using the adaptive focus control (AFC)
479 and closed-loop focus system of the DMi8 microscope. To quantify non-lysed cells, phase-
480 contrast images were analyzed using the plugin MicrobeJ (51) in ImageJ (52). The default
481 MicrobeJ settings were used for cell segmentation (Fit shape, rod-shaped bacteria) apart from
482 the following settings: area: 1-max µm; length: 2.5–20 µm; width: 0.4–2 µm; curvature 0.0–
483 0.15, angularity 0.0–0.25 and intensity 0.0–2000.

484 **T5 bacteriophage adsorption assay**

485 Adsorption assays were performed as previously described (53). *E. coli* wild type and
486 Δ*rlmF*Δ*rlmJ* mutant were grown as described above and infected with T5 phage at an MOI of
487 0.1. Free phages were sampled immediately post-infection (0 min), then every 5 min for 30 min
488 using 0.22-µm sterile filtration. Plaque assays (47) were performed as described above to
489 enumerate the free phage concentration.

490 **One-step growth curve**

491 One-step growth curves were performed as described previously (48, 54). *E. coli* wild type and
492 Δ*rlmF*Δ*rlmJ* mutant were grown as described above, infected with T5 phage at an MOI of 0.001
493 and incubated at 37 °C for 10 min. After initial adsorption, the remaining free phages were
494 removed via centrifugation (5000 × *g*, 5 min, 4 °C) and the pellet was resuspended in fresh pre-
495 warmed Nutrient broth. Samples were incubated at 37 °C with shaking and collected (including
496 t = 0) at 10-min intervals over 30 min, followed by 5-min intervals up to 105 min. Plaque assays
497 (47) were performed as described above immediately after sample collection.

498 **Statistical analysis and data presentation**

499 All numerical data were analyzed and graphs were prepared with GraphPad Prism version
500 10.0.2 (GraphPad Software, La Jolla, CA, USA). Statistics were performed using paired and
501 unpaired Student´s *t*-test. Microscopy images were prepared from a total of 2,080 *E. coli* wild
502 type and 1,923 Δ*rlmF*Δ*rlmJ* mutant cells and analyzed with MicrobeJ. All figures were
503 generated using Affinity Designer version 2.2.1 (Serif, West Bridgford, UK).

504 All experiments were repeated at least three times to ensure reproducibility.

505

506 ## Acknowledgements

507 We thank Korinna Burdack and Inès Wullkopf for conducting plaque assays, Dimitar Petrov
508 for isolating RNA, and Siobhan Cusack for proofreading the manuscript. B.S. acknowledges
509 the support of the Graduate School Life Science Munich (LSM).

510 This work was financially supported by the Deutsche Forschungsgemeinschaft (DFG, German
511 Research Foundation): Project numbers 464582101 (JU270/21-1; BR6622/1-1) and 325871075
512 (SFB 1309).

513 B.S., S.B. and K.J. conceptualized the study. B.S., S.B., T.C., S.R. and K.J. designed the
514 methodology. B.S. performed the investigation. B.S., S.B. and K.J. wrote the original draft,
515 B.S., S.B., T.C., S.R. and K.J. reviewed and edited the manuscript. K.J. and S.B. acquired
516 funding, provided resources, and supervised the study.

517 ## Data availability

518 Additional information required to reanalyze the data reported in this paper is available from
519 the lead contacts upon request.

520

521 ## References

522 1. Wilkinson E, Cui Y-H, He Y-Y. 2022. Roles of RNA modifications in diverse cellular
523 functions. Front Cell Dev Biol 10:828683.

524 2. Fu Y, Dominissini D, Rechavi G, He C. 2014. Gene expression regulation mediated through
525 reversible m^{6}A RNA methylation. Nature reviews Genetics 15:293–306.

526 3. Meyer KD, Jaffrey SR. 2014. The dynamic epitranscriptome: *N*^{6}-methyladenosine and gene
527 expression control. Nat Rev Mol Cell Biol 15:313–326.

528 4. Baquero-Pérez B, Yonchev ID, Delgado-Tejedor A, Medina R, Puig-Torrents M, Sudbery I,
529 Begik O, Wilson SA, Novoa EM, Díez J. 2024. *N*^{6}-methyladenosine modification is not a
530 general trait of viral RNA genomes. Nat Commun 15:1964.

531 5. He H, Jia M, Liu J, Zhou X, Li F. 2023. Roles of RNA m^{6}A modifications in plant-virus
532 interactions. Stress Biol 3:57.

533 6. Zhang X, Peng Q, Wang L. 2023. *N*^{6}-methyladenosine modification—a key player in viral
534 infection. Cell Mol Biol Lett 28:78.

535 7. Li H, Guo Y, Qi W, Liao M. 2022. *N*^{6}-methyladenosine modification of viral RNA and its
536 role during the recognition process of RIG-I-like receptors. Front Immunol 13:1031200.

537 8. Batinovic S, Wassef F, Knowler SA, Rice DTF, Stanton CR, Rose J, Tucci J, Nittami T, Vinh
538 A, Drummond GR, Sobey CG, Chan HT, Seviour RJ, Petrovski S, Franks AE. 2019.
539 Bacteriophages in natural and artificial environments. Pathogens 8:100.

540 9. Salmond GPC, Fineran PC. 2015. A century of the phage: past, present and future. Nat Rev
541 Microbiol 13:777–786.

542 10. Yang JY, Fang W, Miranda-Sanchez F, Brown JM, Kauffman KM, Acevero CM, Bartel
543 DP, Polz MF, Kelly L. 2021. Degradation of host translational machinery drives tRNA
544 acquisition in viruses. Cell Syst 12:771-779.e5.

545 11. Vassallo CN, Doering CR, Laub MT. 2024. Anti-viral defense by an ADP-
546 ribosyltransferase that targets mRNA to block translation. bioRxiv 2024.02.24.581662.

547 12. Petrov DP, Kaiser S, Kaiser S, Jung K. 2022. Opportunities and challenges to profile mRNA
548 modifications in *Escherichia coli*. Chembiochem 23:e202200270.

549 13. Sergiev PV, Serebryakova MV, Bogdanov AA, Dontsova OA. 2008. The *ybiN* gene of
550 *Escherichia coli* encodes adenine-N^6 methyltransferase specific for modification of A1618 of
551 23 S ribosomal RNA, a methylated residue located close to the ribosomal exit tunnel. J Mol
552 Biol 375:291–300.

553 14. Golovina AY, Dzama MM, Osterman IA, Sergiev PV, Serebryakova MV, Bogdanov AA,
554 Dontsova OA. 2012. The last rRNA methyltransferase of *E. coli* revealed: the *yhiR* gene
555 encodes adenine-N^6 methyltransferase specific for modification of A2030 of 23S ribosomal
556 RNA. RNA (New York, NY) 18:1725–1734.

557 15. Golovina AY, Sergiev PV, Golovin AV, Serebryakova MV, Demina I, Govorun VM,
558 Dontsova OA. 2009. The *yfiC* gene of *E. coli* encodes an adenine-N^6 methyltransferase that
559 specifically modifies A37 of $tRNA_1^{Val}$(cmo^5UAC). RNA (New York, NY) 15:1134–41.

560 16. Breger K, Kunkler CN, O'Leary NJ, Hulewicz JP, Brown JA. 2024. Ghost authors revealed:
561 The structure and function of human N^6-methyladenosine RNA methyltransferases. Wiley
562 Interdiscip Rev: RNA 15:e1810.

563 17. Pletnev P, Guseva E, Zanina A, Evfratov S, Dzama M, Treshin V, Pogorel'skaya A,
564 Osterman I, Golovina A, Rubtsova M, Serebryakova M, Pobeguts OV, Govorun VM,
565 Bogdanov AA, Dontsova OA, Sergiev PV. 2020. Comprehensive functional analysis of
566 *Escherichia coli* ribosomal RNA methyltransferases. Front Genet 11:97.

567 18. Lin B, Wang Z, Malanoski AP, O'Grady EA, Wimpee CF, Vuddhakul V, Jr NA, Thompson
568 FL, Gomez-Gil B, Vora GJ. 2010. Comparative genomic analyses identify the *Vibrio harveyi*
569 genome sequenced strains BAA-1116 and HY01 as *Vibrio campbellii*. Environ Microbiol Rep
570 2:81–89.

571 19. Lorenz N, Reiger M, Toro-Nahuelpan M, Brachmann A, Poettinger L, Plener L, Lassak J,
572 Jung K. 2016. Identification and initial characterization of prophages in *Vibrio campbellii*.
573 PLoS ONE 11:e0156010.

574 20. Wendling CC, Refardt D, Hall AR. 2021. Fitness benefits to bacteria of carrying prophages
575 and prophage-encoded antibiotic-resistance genes peak in different environments. Evol Int J
576 Org Evol 75:515–528.

577 21. Droubogiannis S, Katharios P. 2022. Genomic and biological profile of a novel
578 bacteriophage, Vibrio phage Virtus, which improves survival of *Sparus aurata* larvae
579 challenged with *Vibrio harveyi*. Pathogens 11:630.

580 22. Blattner FR, III GP, Bloch CA, Perna NT, Burland V, Riley M, Collado-Vides J, Glasner
581 JD, Rode CK, Mayhew GF, Gregor J, Davis NW, Kirkpatrick HA, Goeden MA, Rose DJ, Mau
582 B, Shao Y. 1997. The complete genome sequence of *Escherichia coli* K-12. Science 277:1453–
583 1462.

584 23. Demerec M, Fano U. 1945. Bacteriophage-resistant mutants in *Escherichia coli*. Genetics
585 30:119–136.

586 24. Riquelme-Barrios S, Camus LV, Cusack SA, Burdack K, Petrov DP, Yesiltac N, Kaiser S,
587 Giehr P, Jung K. 2024. Decoding the *Escherichia coli* epitranscriptome. in preparation.

588 25. Kutter E. 2009. Bacteriophages. Methods Mol Biol 141–149.

589 26. Abedon ST. 2000. The murky origin of snow white and her T-even dwarfs. Genetics
590 155:481–6.

591 27. Casjens SR, Hendrix RW. 2015. Bacteriophage lambda: Early pioneer and still relevant.
592 Virology 479:310–330.

593 28. Ackermann H-W. 1998. Tailed bacteriophages: The order Caudovirales. Adv Virus Res
594 51:135–201.

595 29. Silva JB, Storms Z, Sauvageau D. 2016. Host receptors for bacteriophage adsorption. FEMS
596 Microbiol Lett 363:fnw002.

597 30. Li J, Ding J, Chen M, Chen K, Zou Y, Xu X, Zhang D, Yu X, Ding Z. 2023. Transcriptome-
598 wide N^6-methyladenosine modification profiling of mRNAs during infection of Newcastle
599 disease virus in chicken macrophages. Virus Res 323:198993.

600 31. Pozhydaieva N, Wolfram-Schauerte M, Keuthen H, Höfer K. 2024. The enigmatic
601 epitranscriptome of bacteriophages: putative RNA modifications in viral infections. Curr Opin
602 Microbiol 77:102417.

603 32. Depping R, Lohaus C, Meyer HE, Rüger W. 2005. The mono-ADP-ribosyltransferases Alt
604 and ModB of bacteriophage T4: Target proteins identified. Biochem Biophys Res Commun
605 335:1217–1223.

606 33. Tiemann B, Depping R, Gineikiene E, Kaliniene L, Nivinskas R, Rüger W. 2004. ModA
607 and ModB, two ADP-ribosyltransferases encoded by bacteriophage T4: catalytic properties and
608 mutation analysis. J Bacteriol 186:7262–7272.

609 34. Wolfram-Schauerte M, Pozhydaieva N, Grawenhoff J, Welp LM, Silbern I, Wulf A, Billau
610 FA, Glatter T, Urlaub H, Jäschke A, Höfer K. 2023. A viral ADP-ribosyltransferase attaches
611 RNA chains to host proteins. Nature 620:1054–1062.

612 35. Tsai K, Flemington EK, Courtney DG, Cullen BR. 2018. Addition of m^6A to SV40 late
613 mRNAs enhances viral structural gene expression and replication. PLoS Pathogens
614 14:e1006919.

615 36. Castillo D, D'Alvise P, Middelboe M, Gram L, Liu S, Kalatzis PG, Kokkari C, Katharios
616 P. 2015. Draft genome sequences of the fish pathogen *Vibrio harveyi* strains VH2 and VH5.
617 Genome Announc 3:e01062-15.

618 37. Studier FW, Moffatt BA. 1986. Use of bacteriophage T7 RNA polymerase to direct
619 selective high-level expression of cloned genes. J Mol Biol 189:113–130.

620 38. Macinga DR, Parojcic MM, Rather PN. 1995. Identification and analysis of *aarP*, a
621 transcriptional activator of the 2'-N-acetyltransferase in *Providencia stuartii*. J Bacteriol
622 177:3407–3413.

623 39. Murray NE, Brammar WJ, Murray K. 1977. Lambdoid phages that simplify the recovery
624 of *in vitro* recombinants. Mol Gen Genet 150:53–61.

625 40. Lassak J, Henche A-L, Binnenkade L, Thormann KM. 2010. ArcS, the cognate sensor
626 kinase in an atypical Arc system of *Shewanella oneidensis* MR-1. Appl Environ Microbiol
627 76:3263–3274.

628 41. Gibson DG, Young L, Chuang R-Y, Venter JC, Hutchison CA, Smith HO. 2009. Enzymatic
629 assembly of DNA molecules up to several hundred kilobases. Nat Methods 6:343–345.

630 42. Schwarz J, Brameyer S, Hoyer E, Jung K. 2023. The interplay of AphB and CadC to activate
631 acid resistance of *Vibrio campbellii*. J Bacteriol 205:e00457-22.

632 43. Laemmli UK. 1970. Cleavage of structural proteins during the assembly of the head of
633 bacteriophage T4. Nature 227:680–685.

634 44. Lu Y, Jia R, Zhang Z, Wang M, Xu Y, Zhu D, Chen S, Liu M, Yin Z, Chen X, Cheng A.
635 2014. *In vitro* expression and development of indirect ELISA for capsid protein of duck
636 circovirus without nuclear localization signal. Int J Clin Exp Pathol 7:4938–44.

637 45. Andreolla AP, Erpen LMS, Frandoloso R, Kreutz LC. 2018. Development of an indirect
638 ELISA based on recombinant capsid protein to detect antibodies to bovine leukemia virus. Braz
639 J Microbiol 49:68–75.

640 46. Fortier, Moineau L-C and, Sylvain. 2009. Phage production and maintenance of stocks,
641 including expected stock lifetimes Methods Mol Biol 501:203-19.

642 47. Kropinski AM, Mazzocco A, Waddell TE, Lingohr E, Johnson RP. 2009. Enumeration of
643 bacteriophages by double agar overlay plaque assay. Methods Mol Biol 501:69-76.

644 48. Brandão A, Pires DP, Coppens L, Voet M, Lavigne R, Azeredo J. 2021. Differential
645 transcription profiling of the phage LUZ19 infection process in different growth media. RNA
646 Biol 18:1778–1790.

647 49. Melo LDR, Monteiro R, Pires DP, Azeredo J. 2022. Phage-host interaction analysis by flow
648 cytometry allows for rapid and efficient screening of phages. Antibiotics 11:164.

649 50. Mandal PK, Ballerin G, Nolan LM, Petty NK, Whitchurch CB. 2021. Bacteriophage
650 infection of *Escherichia coli* leads to the formation of membrane vesicles via both explosive
651 cell lysis and membrane blebbing. Microbiology 167:001021.

652 51. Ducret A, Quardokus EM, Brun YV. 2016. MicrobeJ, a tool for high throughput bacterial
653 cell detection and quantitative analysis. Nat Microbiol 1:16077–14.

654 52. Schneider CA, Rasband WS, Eliceiri KW. 2012. NIH Image to ImageJ: 25 years of image
655 analysis. Nat Methods 9:671–675.

656 53. Howard-Varona C, Hargreaves KR, Solonenko NE, Markillie LM, White RA, Brewer HM,
657 Ansong C, Orr G, Adkins JN, Sullivan MB. 2018. Multiple mechanisms drive phage infection
658 efficiency in nearly identical hosts. ISME J 12:1605–1618.

659 54. Duarte J, Pereira C, Costa P, Almeida A. 2021. Bacteriophages with potential to inactivate
660 *Aeromonas hydrophila* in Cockles: *In vitro* and *in vivo* preliminary studies. Antibiotics 10:710.